

# Self-Supervised Learning with a Multi-Task Latent Space Objective

Pierre-François De Plaen<sup>1</sup> Abhishek Jha<sup>2,\*</sup> Luc Van Gool<sup>1,3,4,5</sup>

Tinne Tuytelaars<sup>1</sup> Marc Proesmans<sup>1,5</sup>

<sup>1</sup>ESAT-PSI, KU Leuven, Belgium <sup>2</sup>VIB.AI, KU Leuven, Belgium

<sup>3</sup>CVL, ETH Zürich, Switzerland <sup>4</sup>INSAIT, Sofia University, Bulgaria <sup>5</sup>TRACE vzw

## Abstract

*Self-supervised learning (SSL) methods based on Siamese networks learn visual representations by aligning different views of the same image. The multi-crop strategy, which incorporates small local crops to global ones, enhances many SSL frameworks but causes instability in predictor-based architectures such as BYOL, SimSiam, and MoCo v3. We trace this failure to the shared predictor used across all views and demonstrate that assigning a separate predictor to each view type stabilizes multi-crop training, resulting in significant performance gains. Extending this idea, we treat each spatial transformation as a distinct alignment task and add cutout views, where part of the image is masked before encoding. This yields a simple multi-task formulation of asymmetric Siamese SSL that combines global, local, and masked views into a single framework. The approach is stable, generally applicable across backbones, and consistently improves the performance of ResNet and ViT models on ImageNet.*

## 1. Introduction

Self-supervised learning (SSL) has become a dominant paradigm for learning visual representations without supervision. It builds training signals directly from data, allowing models to discover visual structure on their own. Among SSL approaches, Siamese-based methods, often referred to as Joint Embedding Architectures [9, 10, 25, 28, 60], have proven especially effective. They learn by aligning representations of different augmented views of the same image. Recent large-scale efforts [43, 45] have further advanced this paradigm by leveraging larger datasets and more powerful architectures, yielding representations with remarkable generalization across a wide range of visual tasks.

\*Part of this work was conducted while Abhishek was affiliated with ESAT-PSI, KU Leuven, Belgium.

Code: <https://github.com/pfdp0/mulan>

An important factor behind this progress is the multi-crop strategy, which adds several small local crops to the standard pair of global views. This simple idea promotes spatial consistency and has been crucial to the success of clustering-based methods, such as SwAV [8] and DINO [9]. Yet, it turns out to be unstable in predictor-based Siamese architectures, such as BYOL [25], SimSiam [11], and MoCo v3 [13], where the online and target branches play different roles, with the former including a prediction head. This instability has prevented these otherwise strong frameworks from benefiting from one of the most effective SSL augmentations.

We analyze this limitation and trace it to the shared predictor used across all views. A single predictor must align representations from both global and local crops, which differ strongly in scale and content, leading to unstable optimization. We resolve this by assigning a dedicated predictor to each view type, while keeping the encoder shared (Fig. 1b). This simple modification stabilizes multi-crop training, yielding consistent accuracy gains across asymmetric frameworks. On ImageNet, it improves BYOL by +4% in linear evaluation, and provides similar gains for SimSiam and MoCo v3 (Tab. 1).

With multi-crop stabilized, we turn to the question of how to extend it. Prior work [10, 25, 40, 47] and our analysis (Sec. 5.2) show that spatial augmentations contribute most to representation quality. This suggests that spatial augmentations are the most promising direction for extending multi-crop. We therefore add cutout [17] views into multi-crop, where a random region of the image is masked before encoding. Random cutout removes internal content rather than external context, complementing local crops and encouraging the model to infer missing information from surrounding regions. This naturally connects Siamese SSL to masked image modeling [2, 14, 29], while remaining simple and not tied to a specific backbone.

Together, these elements define a unified and stable framework for asymmetric Siamese SSL (Fig. 1c). Each spatial transformation (global, local, or cutout) defines a distinct task with its own predictor. All tasks share the same

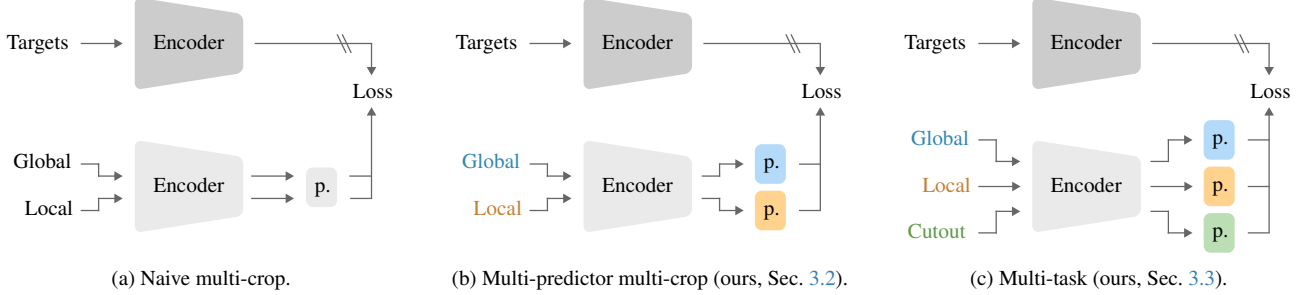


Figure 1. Overview of our predictor-based Siamese SSL framework. Naive multi-crop (left) is unstable under a shared predictor. Using one predictor per view type (middle) stabilizes training. Adding cutout views (right) yields a simple multi-task formulation that further improves downstream performance. Here,  $p.$  denotes a predictor, and colors indicate distinct predictors.

encoder (i.e., backbone and projection head) and alignment loss, forming a simple multi-task view of Siamese SSL compatible with both CNN and transformer backbones.

In summary, our contributions are the following:

1. We identify the shared predictor as the primary cause of multi-crop instability in asymmetric Siamese SSL and show that assigning view-specific predictors enables these methods to benefit from the multi-crop strategy.
2. Building on this stable setup, we extend the model with cutout views, which have a complementary training signal to cropped views. Our analyses suggest that spatial augmentations, including cropping and asymmetric cutout, are the most effective source of supervision in self-supervised learning.
3. We validate the approach on key asymmetric architectures (BYOL, SimSiam, and MoCo v3) with both ResNet and ViT backbones, achieving consistent gains on ImageNet under linear and kNN evaluation.

## 2. Related Work

**Self-Supervised Learning.** Early work in visual self-supervised learning (SSL) focused on handcrafted pretext tasks that required solving spatial or contextual prediction problems, including inpainting [44], jigsaw puzzles [42], relative patch prediction [19], rotation prediction [23], and colorization [63]. These methods demonstrated that purely spatial supervision can yield semantically meaningful representations without labels. This perspective remains relevant to our approach, which leverages asymmetric cutout as a lightweight spatial latent space task.

Subsequent work shifted toward invariance-based objectives. Contrastive approaches such as SimCLR [10] and MoCo [28] align augmented views while repelling different images, while clustering-based methods like DeepCluster [7] and SwAV [8] replace instance discrimination with prototype assignments. In parallel, non-contrastive methods avoid negatives by explicitly enforcing feature diversity through decorrelation or variance constraints, as in Barlow

Twins [60], VICReg [6], W-MSE [21], and ADM [15].

Masked image modeling (MIM) constitutes another major direction, training models to reconstruct masked content either in pixel space [29, 56] or at the token level [5]. Hybrid approaches such as MSN [1] and iBOT [66] further unify masked prediction with prototype-based or distillation objectives, primarily in ViT-based settings [2, 14]. While these works broaden the SSL design space, our focus is on improving predictor-based Siamese architectures in a backbone-agnostic manner.

**Predictor-based Siamese SSL.** Predictor-based Siamese methods such as BYOL [25] and SimSiam [11] showed that strong representations can be learned using a single invariance loss, without negatives, clustering, or reconstruction. Collapse is avoided through architectural asymmetry, typically via an online-target encoder pair and a predictor on the online branch. MoCo v3 [13] extended this paradigm to Vision Transformers [20], demonstrating the benefits of asymmetry even in contrastive formulations.

Teacher-student approaches such as DINO [9] and iBOT [66] also rely on online-target asymmetry with EMA updates, but omit a predictor head and instead stabilize training through centroid-based probability targets, or a centering and sharpening mechanism.

While predictor-based methods are stable in the two-crop regime, naively extending them to multi-crop often leads to instability [3, 9, 39, 40]. Prior work proposed addressing this issue via auxiliary regularization [64]. In contrast, we show that the shared predictor itself is the source of instability: assigning one predictor per view type stabilizes multi-crop training without modifying the backbone or alignment loss.

**Data Augmentations and Spatial Views in SSL.** Data augmentations are central in Siamese SSL because they define the proxy task. Cropping is particularly powerful, as it promotes spatial correspondence across views and is re-

sponsible for most of the accuracy gains [25, 40, 41]. The multi-crop strategy introduced in SwAV [8] and adopted in DINO [9] enriches supervision with local views, but poses challenges for predictor-based methods.

Several other approaches explicitly leveraged local features [33, 52, 54, 55]: they imposed region- or pixel-level consistency through additional losses or dense contrastive objectives. In contrast, our method follows SwAV and operates solely on final representations, introducing global-local consistency through augmentations rather than multi-level or dense supervision.

Recent masked-prediction frameworks such as I-JEPA [2] and CAPI [14] further demonstrated that spatial prediction alone can yield strong semantic features with minimal augmentations. Inspired by these findings, we introduce asymmetric cutout views as a complementary spatial prediction task within Siamese SSL.

In parallel, cutout-style perturbations, including random erasing, mixup, CutMix, and object-centric cropping, have been widely used to regularize supervised and self-supervised learning [38, 59, 62, 65]. In this work, we focus specifically on cutout as a form of within-image occlusion that isolates spatial masking effects without mixing images or labels, making it a simple building block for our method.

**Multi-Task SSL.** Combining multiple pretext tasks has long been known to improve representation quality. Early work by Doersch & Zisserman [18] showed that combining heterogeneous pretext signals in a single backbone is beneficial, even with a simple multi-head setup, and similar findings were reported for 3D point clouds, where multiple self-supervised objectives (clustering, reconstruction, self-labeling) were jointly optimized on a shared encoder [26]. Beyond images and point clouds, multi-task self-supervision has also been explored for skeleton-based action recognition, where several complementary pretext tasks share a common trunk but use dedicated task-specific heads [36]. With the emergence of transformer-based masked modeling, multi-tasking became tightly coupled with multi-modality: Multimodal MAE variants [4, 22] demonstrated that a unified ViT encoder can reconstruct several targets (RGB, depth, segmentation, language) from masked inputs, and RGB-D-centric methods such as Co-MAE [57] or the progressive contrastive-MAE-denoising scheme of [31] further showed that sequencing contrastive alignment and masked reconstruction can boost transfer on small RGB-D datasets. However, most of these approaches are tailored to generative or reconstruction-style SSL, or rely on modality- or task-specific decoding. In contrast, we remain entirely in latent space and show that multi-tasking arises naturally once different spatial views must be aligned.

Closer to our setting, adaptive multi-head contrastive learning [51] and multi-target BYOL [46] introduced archi-

tectural branching to accommodate heterogeneous views. However, they neither introduce additional predictors nor address the instability of predictor-based Siamese SSL under multi-crop. Our approach instead assigns a dedicated predictor to each view type while keeping the backbone, projector, and alignment loss shared, enabling stable multi-crop training and effective integration of multiple spatial tasks.

## 3. Method

### 3.1. Background

Siamese self-supervised methods learn by aligning representations of different augmented views of the same image. Two identical encoders with shared weights process the views, and a small projection head maps backbone outputs to the representation space used for the loss. Including this projector improves representation quality [10].

Early methods, such as SimCLR [10], used contrastive objectives combining an alignment term with a repulsive term to prevent trivial solutions like collapsed representations. Later approaches, including BYOL [25] and SimSiam [11], eliminated the need for explicit negatives. They introduced asymmetry by assigning different roles to the two branches: the online branch includes a predictor trained by gradient descent, while the target branch is not directly optimized and omits the predictor. In BYOL, target parameters are updated as an exponential moving average of the online ones; in SimSiam, the target is a stop-gradient copy of the online network with shared weights.

### 3.2. Understanding and Stabilizing Multi-Crop

The multi-crop strategy extends the standard two-view setup by introducing several smaller local crops in addition to the usual global views. Each crop is encoded independently, and the model learns to align local representations with their corresponding global ones. This encourages consistency across scales and contextual levels.

Multi-crop significantly improves the performance of many self-supervised learning methods, including contrastive frameworks such as SimCLR [10] and MoCo [28], as well as clustering-based approaches like SwAV [8] and DINO [9]. However, this improvement is not universal. In predictor-based architectures such as BYOL [25], SimSiam [11], and MoCo v3 [13], multi-crop leads to training instability and degraded performance compared to their standard baselines [3, 9, 39, 40].

Caron *et al.* [9] reported this issue for BYOL with a ViT-S backbone: the multi-crop variant achieved only 64.8% accuracy, compared to 71.4% for the two-view baseline. They observed that the transfer accuracy plateaus prematurely and then declines. Reducing the learning rate can avoid the performance break point, but the final accuracy

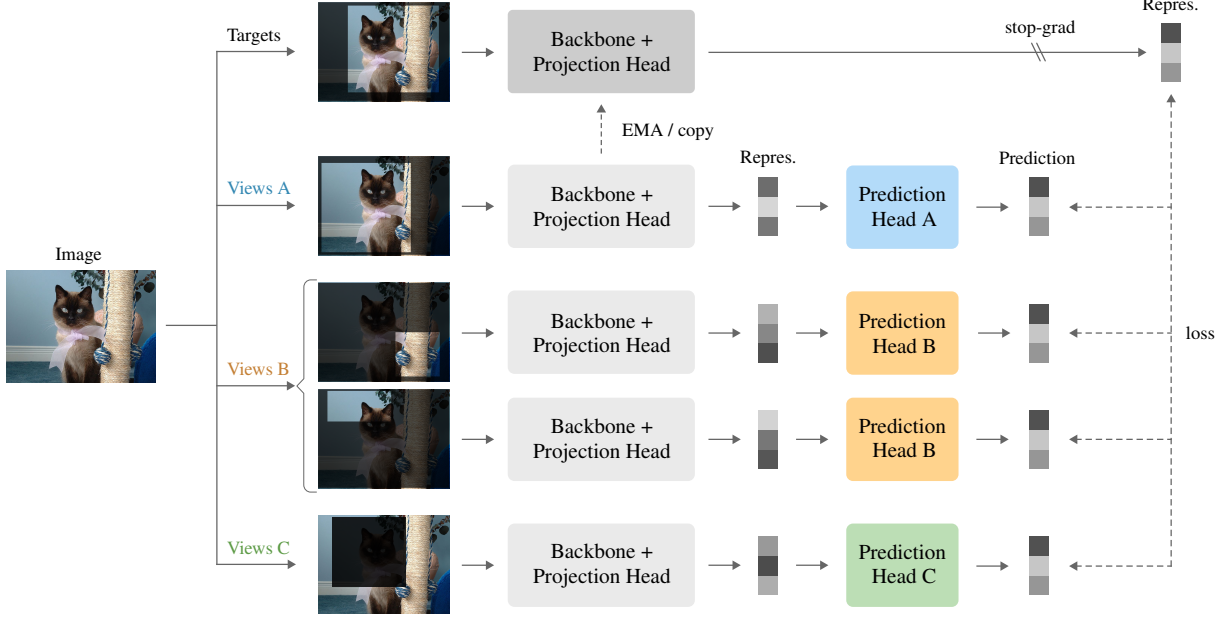


Figure 2. Overview of the proposed framework. Each image is augmented into multiple spatial views: global (views A), local (views B), and cutout (views C). A shared encoder, comprising a backbone and a projection head, extracts features for all views. View-specific prediction heads then generate predictions for each view type. All spatial alignment tasks are optimized jointly under a shared alignment objective. Image from ImageNet validation set (№43632).

remains lower than that obtained without multi-crop training; a similar behavior was observed with a ResNet-50 backbone. Morningstar *et al.* [40] reported analogous findings for MoCo v3, where performance drops by 1.5% with multi-crop, primarily because many runs exhibit training instability. While reducing the batch size mitigates these failures, it again yields models that underperform the standard two-view baseline.

To understand this limitation, we analyze the MoCo family. Multi-crop brings gains in MoCo v2 [12, 40] but degrades performance in MoCo v3 [40, 53]. The key architectural differences between these versions are the removal of the memory bank and the introduction of BYOL-style asymmetry, which includes a predictor on the online branch and an exponential moving average (EMA) target. Since BYOL and MoCo v3 differ only in their loss objectives, this comparison suggests that the asymmetric predictor is the likely source of instability.

To address this, we assign a separate predictor to each view type while keeping the encoder (i.e., backbone and projection head) shared (see Fig. 2). Each predictor specializes in its own kind of views, thereby reducing interference between global and local alignment objectives. This modification does not alter the loss function or require new hyperparameters, and only marginally increases the number of learnable parameters. It isolates predictors by view, resulting in stable optimization across different architectures.

This stabilized formulation enables predictor-based

Siamese methods to effectively exploit multi-crop augmentations (see Sec. 4.1) and serves as the foundation for the spatial prediction framework described next.

### 3.3. Extending Multi-Crop with Cutout Views

Once the multi-crop strategy is stable, we can explore additional transformations. Prior work [10, 40, 47] and our analyses (see Sec. 5.2) suggest that spatial augmentations provide the strongest learning signal in Siamese SSL. We therefore introduce an additional view type, cutout [17], which randomly masks a random rectangular region of the image before encoding.

While local crops most often remove outer context, cutout occludes part of the inner content, making the two augmentations complementary: local crops promote scale invariance, whereas cutout encourages robustness to partial occlusions.

We apply it asymmetrically (see Fig. 3): the online branch sees the masked view, while the target view remains complete. In this setup, the online model is trained to predict the image representation as if it were not masked, thereby encouraging the model to infer missing information from visible regions, forming a simple inpainting-like prediction task.

Based on the stabilized multi-crop design, we use a separate predictor for each view type, while keeping the backbone and projector shared. Formally, let  $z^v$  denote the representation of view type  $v \in \{\text{glob, loc, cutout}\}$ . The total

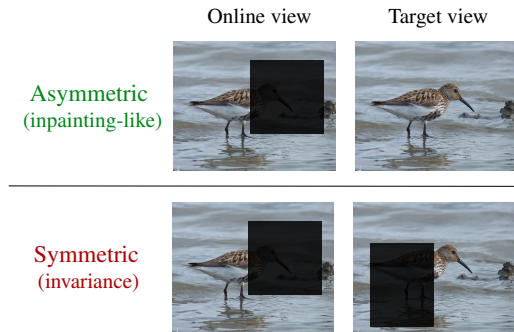


Figure 3. Asymmetric and symmetric cutout. Image from ImageNet validation set (Nº7011).

alignment loss is computed as a weighted sum over view types:

$$\mathcal{L} = \sum_v \lambda_v \mathbb{E} \left[ \|q_v(z_v) - z_{\text{glob}}\|_2^2 \right] \quad (1)$$

where  $q_v$  denotes the predictor for view type  $v$  and  $\lambda_v$  its relative weight. In practice, we equally weight all view types:  $\lambda_{\text{glob}} = \lambda_{\text{loc}} = \lambda_{\text{cutout}}$ .

This formulation treats each spatial transformation as a separate latent space task, unified under a single encoder and alignment objective. It extends predictor-based Siamese SSL from two-view alignment to a multi-task framework that integrates global, local, and cutout views within a single, stable training recipe.

## 4. Experiments

### 4.1. Validation of Multi-Predictor Multi-Crop

We first validate our solution to the instability of multi-crop training in predictor-based Siamese frameworks. As discussed in Sec. 3.2, a shared predictor must align representations from both global and local crops, often causing instability. To address this, we assign a separate predictor to each view type while keeping the encoder shared, and train BYOL, SimSiam, and MoCo v3 under identical settings.

**Setup.** All experiments use a ResNet-50 [27] backbone and follow the original training recipes of each method, except that batch sizes are reduced to 1024 for BYOL and MoCo v3<sup>1</sup>. Models are trained for 200 epochs on ImageNet-1k [16] with standard augmentations. We use two global and four local views. The only modification is the introduction of view-specific predictors; all other hyperparameters remain unchanged.

**Evaluation protocols.** Representation quality is measured using (1) linear evaluation, where a linear classifier

is trained on frozen backbone features, and (2) non-parametric  $k$ -nearest neighbor (kNN) evaluation on the embedding space.

**Results.** Tab. 1 reports linear and kNN accuracies. Introducing view-specific predictors lets all three frameworks benefit from multi-crop training. In BYOL, linear accuracy rises from 70.7% to 74.7%. SimSiam and MoCo v3 show similar gains of around +4 points each. All runs converge reliably at standard learning rates, confirming that the shared predictor was the main source of instability.

Method	Top-1 acc. [%]			
	kNN	$\Delta$	lin.	$\Delta$
BYOL	63.1		70.7	
w. multi-predictor m-c	<b>69.5</b>	<b>+6.4</b>	<b>74.7</b>	<b>+4.0</b>
SimSiam	60.2		69.9	
w. multi-predictor m-c	<b>65.3</b>	<b>+4.9</b>	<b>73.9</b>	<b>+4.0</b>
MoCo v3	64.5		71.4	
w. multi-predictor m-c	<b>68.5</b>	<b>+4.0</b>	<b>75.2</b>	<b>+3.8</b>

Table 1. Downstream performance of self-supervised ResNet-50 models trained with the updated multi-crop (m-c) formulation. All models are pre-trained for 200 epochs.

These results demonstrate that predictor-based SSL methods can fully benefit from multi-crop augmentations once predictors are decoupled by view type. The modification is lightweight, requires no changes to the loss, and generalizes across frameworks.

### 4.2. Effect of Asymmetric Cutout

Before adding cutout views to multi-crop, we first study whether random cutout alone provides a valuable learning signal. We train BYOL using cutout as the only augmentation, masking a random rectangular region in the online view while keeping the target view complete. After 100 epochs on ImageNet, this simple setup reaches 46.8% top-1 accuracy, confirming that the model can learn meaningful representations by predicting the embedding of a full image from a partially masked view.

We then compare asymmetric and symmetric masking. When both views are masked, the model reaches close to random performance (3.4%). This confirms that asymmetry is crucial: the model must infer missing information from an unmasked reference rather than from another incomplete view. These results validate cutout as a viable spatial prediction task and motivate its integration within stabilized multi-crop training in our final multi-task formulation.

### 4.3. Multi-Task Formulation Validation

We now evaluate whether the proposed multi-task formulation (Sec. 3.3) provides benefits beyond the stabilized multi-

<sup>1</sup>This allows training on a single 4-GPU node, with only marginal impact on accuracy.

crop setup (Sec. 3.2). The multi-task design adds random cutout as a new view-type, thereby increasing the diversity of training signals. This experiment investigates whether models can leverage this additional spatial variation to enhance representation quality. We apply the multi-task formulation to BYOL, SimSiam, and MoCo v3, and compare each to its multi-predictor multi-crop baseline under matched compute.

**Implementation details.** We pre-train ResNet-50 backbones following the official training recipes of each method (see App. A for full settings). For a fair comparison, we adjust the number and type of views so that total computational cost remains similar (see App. C); specifically, two local views are replaced with a single cutout view, since local views require roughly half the computation. The effect of view composition is analyzed in the ablation studies (Sec. 5.1). All models are pre-trained for 200 epochs.

**Results.** Tab. 2 shows that adding cutout views further improves the performance of the multi-crop BYOL and SimSiam frameworks by a significant margin, and marginally helps for MoCo v3. Despite being trained for only 200 epochs, all three multi-task frameworks already outperform their respective reference models, highlighting the data efficiency of our approach. For example, the original SimSiam achieved 71.3% linear accuracy after 800 epochs, whereas our multi-task variant reaches 74.7% in just 200 epochs, attaining higher performance in roughly half the wall-clock time.

Method	Strategy	Epochs	Top-1 acc. [%]	
			kNN	lin.
BYOL	baseline	1000	68.0	74.3
BYOL	baseline	200	63.1	70.7
	multi-predictor m-c	200	69.5	74.7
	multi-task	200	<b>69.9</b>	<b>75.6</b>
SimSiam	baseline	800	—	71.3
SimSiam	baseline	200	60.2	69.9
	multi-predictor m-c	200	65.3	73.9
	multi-task	200	<b>66.5</b>	<b>74.7</b>
MoCo v3	baseline	1000	68.9	74.6
MoCo v3	baseline	200	64.5	71.4
	multi-predictor m-c	200	68.5	75.2
	multi-task	200	<b>68.7</b>	<b>75.3</b>

Table 2. Downstream performance of self-supervised ResNet-50 models under different augmentation strategies. Gray baselines correspond to the official long-schedule results from the original papers. All other models use a 200-epoch pre-training schedule.

#### 4.4. Comparison with State-of-the-Art Methods

To assess the scalability, competitiveness, and general applicability of our approach across backbones, we train the multi-task BYOL framework on ImageNet-1k [16] using both convolutional and transformer backbones. This experiment evaluates whether the improvements observed at moderate scales (i.e., 200-epoch schedules) persist under standard large-scale self-supervised learning settings, and how our method compares to leading SSL frameworks.

**Implementation details.** We adopt BYOL [25] as the base framework, given its strong results in our 200-epoch experiments. For the **ResNet-50** [27] backbone, we follow the official BYOL configuration: two-layer projector and predictor networks (hidden dimension 4096, output 256), each with intermediate batch normalization [30] and ReLU activations. We pre-train the model for 800 epochs with the LARS optimizer [58], a linearly scaled [24] learning rate ( $lr = 0.4 \times \text{batch\_size}/256$ ), a cosine decay schedule, and a 10-epoch warm-up. The batch size is 1024<sup>1</sup>, and the weight decay is  $1.5 \times 10^{-6}$ , excluding batch normalization and bias parameters. The target network is updated using an EMA of the student weights [35], with the momentum coefficient increasing from 0.996 to 1.0 following a cosine schedule.

For the **ViT-S** and **ViT-B** [20] backbones, we mostly follow the MoCo v3 [13] recipe, except we do not freeze the patch projection layer, as we did not observe stability or performance gains. The projector and predictor mirror the ResNet design, except that the projector has three layers. We pre-train the backbone for 200 epochs using the Adam optimizer [32] with a linearly scaled learning rate (base  $4 \times 10^{-4}$ ), a batch size of 1024, and a weight decay of 0.1 (excluding batch normalization and bias parameters). The EMA base value is set to 0.998.

**Baselines.** We compare our multi-task BYOL to state-of-the-art self-supervised methods. Contrastive and redundancy-reduction approaches include SimCLR [10], the MoCo family [12, 13, 28], ReLIC v2 [48], and Barlow Twins [60]. Clustering methods include SwAV [8] and DINO [9], while non-contrastive methods include BYOL [25], SimSiam [11], and C-BYOL [34]. For ViT-B models, we also report Masked Image Modeling results from BEiT [5], SimMIM [56], MAE [29], and I-JEPA [2].

For reference, we also report supervised baselines for ResNet-50, ViT-S, and ViT-B, trained using the strong training recipes from PyTorch [50] and DeiT [49].

**ImageNet results.** Tab. 3 summarizes the results. Our multi-task BYOL consistently improves upon the original BYOL baseline across both CNN and transformer backbones. With a ResNet-50, it achieves 76.7% linear and

Method	Epochs	Top-1 acc. [%]	
		kNN	Lin.
<i>Backbone: ResNet-50</i>			
supervised	600	—	80.5
SimCLR	1000	60.7	69.3
MoCo v2	800	61.9	71.1
SimSiam	800	—	71.3
Barlow Twins	1000	66.0	73.2
BYOL	1000	68.0 <sup>†</sup>	74.3
MoCo v3	1000	68.9	74.6
SwAV	800	65.7	75.3
DINO	800	67.5	75.3
C-BYOL	1000	—	75.6
ReLIC v2	1600	70.5 <sup>†</sup>	<b>77.1</b>
BYOL multi-task	800	<b>70.9</b>	76.7
<i>Backbone: ViT-S</i>			
supervised	300	—	79.8
BYOL	300	66.6	71.4
MoCo v2	300	64.4	72.7
MoCo v3	300	—	73.4
SwAV	300	66.3	73.5
DINO	800	<b>74.5</b>	<b>77.0</b>
BYOL multi-task	200	69.3	74.0
<i>Backbone: ViT-B</i>			
supervised	300	—	81.8
BEiT*	800	—	56.7
SimMIM*	800	16.1	56.7
MAE*	1600	27.1	68.0
I-JEPA*	600	—	72.9
SimCLR	300	—	73.9
BYOL	300	68.1	73.9
MoCo v3	300	71.4	76.7
DINO	800	<b>76.1</b>	<b>78.2</b>
BYOL multi-task	200	70.6	77.7

Table 3. Evaluation of SSL techniques pre-trained on ImageNet-1k. \*MIM methods. <sup>†</sup>Converted from JAX checkpoints; linear evaluation re-run for verification.

70.9% kNN accuracy, outperforming BYOL by +2.4% and +2.9%, respectively, and surpassing clustering-based methods such as SwAV and DINO. Performance is comparable to ReLIC v2, which attains slightly higher linear accuracy (77.1%) but a lower kNN score (70.5%), indicating similar overall representation quality.

On transformer backbones, the multi-task BYOL also yields substantial gains. With a ViT-S, linear accuracy improves from 71.4% to 74.0%, demonstrating effective transfer to transformers. Scaling to ViT-B, linear accuracy reaches 77.7% (+3.7% over our ViT-S), a larger gain than observed for DINO (+1.2%). While performance remains slightly below DINO, both BYOL and MoCo v3 tend to saturate with long ViT training schedules, suggesting room for further improvement via optimization or regularization.

Finally, our approach outperforms all MIM methods, consistent with findings that MIM models generally require full fine-tuning for strong performance [29, 37].

Overall, these results indicate that the multi-task formulation scales across CNN and transformer backbones of different sizes, consistently improving representation quality.

**Transfer to dense tasks.** We evaluate transfer to COCO object detection and segmentation (Tab. 4) using Mask R-CNN with FPN and a ResNet-50 backbone. Dense tasks require spatially detailed features, providing a complementary assessment of learned representations beyond classification. Our multi-task BYOL outperforms supervised pre-training (41.8 vs. 39.0 AP for detection, 38.0 vs. 35.4 AP for segmentation) and prior SSL methods, achieving the highest AP on both tasks. These results suggest that the multi-task formulation produces representations that generalize well and could be used in a variety of downstream vision tasks.

Method	det. (AP)	segm. (AP)
supervised	39.0	35.4
MoCo v2	39.8	36.1
BYOL	40.4	37.0
SwAV	41.6	37.8
Barlow Twins	40.0	36.7
BYOL multi-task	<b>41.8</b>	<b>38.0</b>

Table 4. Transfer performance (ResNet-50) on COCO using Mask R-CNN with FPN (1× schedule from detectron2).

Finally, we report semi-supervised learning and fine-tuning results in App. B.

	glob.	loc.	cutout	kNN	Lin.
BYOL	2	0	0	63.1	70.7
w. more views	4	0	0	64.3	71.7
w. local views	2	4	0	69.5	74.7
w. cutout views	2	0	2	68.6	73.7
w. multi-task	2	2	1	<b>69.9</b>	<b>75.6</b>

Table 5. Effect of number and type of views on downstream performance. Each view type uses a different prediction head. Models are pre-trained for 200 epochs.

## 5. Ablation Studies

### 5.1. Influence of View Composition

Tab. 5 analyzes how the number and type of views affect BYOL performance. Increasing the number of global views from two to four yields only a modest improvement (70.7% to 71.7%), an effect that would likely diminish with longer

	Spatial augs.			Other augs.				Lin acc.
	crop	cutout	flip	jitter	gray	solar	blur	
Baseline	✓	✗	✓	✓	✓	✓	✓	70.7
Remove crop	✗	✗	✓	✓	✓	✓	✓	33.8
Crop only	✓	✗	✗	✗	✗	✗	✗	55.3
Cutout only	✗	✓	✗	✗	✗	✗	✗	46.8

Table 6. Effect of individual data augmentations on BYOL (ResNet-50). Removing cropping causes a large performance drop, while cropping or asymmetric cutout alone remains competitive. Spatial augmentations outperform all non-spatial combinations. Models are trained for 200 epochs, except the cutout-only variant, which saturates earlier.

training schedules. Introducing new view types instead produces substantial gains: local views raise performance to 74.7%, and global+cutout views reach 73.7%, confirming that view diversity is more valuable than quantity alone.

Notably, the global+cutout configuration significantly outperforms the baseline, suggesting that the benefits of multi-crop strategies can be attributed to the increased spatial diversity, rather than to the inclusion of smaller-resolution crops specifically.

The multi-task configuration achieves the best result with 75.6% linear accuracy despite using fewer total views than the multi-crop setup. This confirms that cutout and local views provide complementary training signals.

## 5.2. On the Importance of Spatial Augmentations

We introduced random cutout as a complementary view type within the multi-crop setting. This choice is motivated by prior evidence and our own findings, which suggest that spatial augmentations play a disproportionately important role in SSL.

Early work by Chen *et al.* [10] showed that strong compositions of augmentations are crucial for contrastive learning, as they define the invariances the model must capture. Subsequent studies challenged this view. Grill *et al.* [25] reported that BYOL maintains competitive accuracy using only random cropping (59.4%), and Moutakanni *et al.* [41] reported similar trends for DINOv2 [43] at scale.

Our ablation results in Tab. 6 confirm this observation. In a 200-epoch schedule, cropping alone yields 55.3% top-1 accuracy on ImageNet, while removing cropping from the full augmentation pipeline reduces accuracy from 70.7% to 33.8%. Additionally, our asymmetric cutout strategy, which masks only the online view, achieves 46.8% accuracy, also outperforming the combination of all non-spatial augmentations. These results suggest that spatial transformations provide the dominant training signal for SSL.

## 6. Conclusion

We investigated why multi-crop, a central component in modern self-supervised learning, often fails in predictor-

based Siamese methods such as BYOL, SimSiam, and MoCo v3. Our analysis traced the failure to the use of a single shared predictor, which is forced to align representations from very different spatial views, often driving the model to collapse.

We addressed this issue by assigning a dedicated predictor for each view type. This simple modification stabilizes training and yields consistent gains across three standard frameworks on ImageNet. Beyond its empirical benefits, this approach offers a clear interpretation of Siamese SSL: each spatial transformation defines a pretext task, and these tasks can be combined effectively within a unified framework.

Building on this, we explored occlusion-based supervision via cutout views, yielding further improvements and highlighting a flexible way to incorporate new spatial supervision signals without modifying the architecture.

In summary, decoupling predictors across view types makes multi-crop effective in predictor-based Siamese SSL and enables the incorporation of additional spatial supervision, such as cutout views. These findings suggest that similar principles could apply to structured modalities such as videos or point clouds, where spatial or geometric transformations may play a similarly central role for pre-training. Another promising direction is to condition the predictors on view-specific information (e.g., cutout coordinates). This modification would transform the model from a standard Siamese or Joint-Embedding Architecture toward a Joint-Embedding Predictive Architecture, shifting the focus from learning invariant features to task-conditional prediction and enabling richer forms of self-supervision.

## Acknowledgments

Most of the computational resources and services used in this work were provided by the VSC (Flemish Supercomputer Center), funded by the Research Foundation Flanders (FWO) and the Flemish Government – department WEWIS.

## References

[1] Mahmoud Assran, Mathilde Caron, Ishan Misra, Piotr Bojanowski, Florian Bordes, Pascal Vincent, Armand Joulin, Mike Rabbat, and Nicolas Ballas. Masked siamese networks for label-efficient learning. In *ECCV*, pages 456–473. Springer, 2022. 2

[2] Mahmoud Assran, Quentin Duval, Ishan Misra, Piotr Bojanowski, Pascal Vincent, Michael Rabbat, Yann LeCun, and Nicolas Ballas. Self-supervised learning from images with a joint-embedding predictive architecture. In *CVPR*, pages 15619–15629, 2023. 1, 2, 3, 6

[3] Arthur Aubret, Céline Teulière, and Jochen Triesch. Seeing the whole in the parts in self-supervised representation learning. *arXiv preprint arXiv:2501.02860*, 2025. 2, 3

[4] Roman Bachmann, David Mizrahi, Andrei Atanov, and Amir Zamir. Multimae: Multi-modal multi-task masked autoencoders. In *ECCV*, pages 348–367. Springer, 2022. 3

[5] Hangbo Bao, Li Dong, Songhao Piao, and Furu Wei. Beit: Bert pre-training of image transformers. In *ICLR*, 2021. 2, 6

[6] Adrien Bardes, Jean Ponce, and Yann LeCun. Vircreg: Variance-invariance-covariance regularization for self-supervised learning. In *ICLR*, 2021. 2

[7] Mathilde Caron, Piotr Bojanowski, Armand Joulin, and Matthijs Douze. Deep clustering for unsupervised learning of visual features. In *ECCV*, pages 132–149, 2018. 2

[8] Mathilde Caron, Ishan Misra, Julien Mairal, Priya Goyal, Piotr Bojanowski, and Armand Joulin. Unsupervised learning of visual features by contrasting cluster assignments. *NeurIPS*, 33:9912–9924, 2020. 1, 2, 3, 6, 12

[9] Mathilde Caron, Hugo Touvron, Ishan Misra, Hervé Jégou, Julien Mairal, Piotr Bojanowski, and Armand Joulin. Emerging properties in self-supervised vision transformers. In *ICCV*, pages 9650–9660, 2021. 1, 2, 3, 6, 12, 13

[10] Ting Chen, Simon Kornblith, Mohammad Norouzi, and Geoffrey Hinton. A simple framework for contrastive learning of visual representations. In *ICML*, pages 1597–1607. PMLR, 2020. 1, 2, 3, 4, 6, 8, 13

[11] Xinlei Chen and Kaiming He. Exploring simple siamese representation learning. In *CVPR*, pages 15750–15758, 2021. 1, 2, 3, 6

[12] Xinlei Chen, Haoqi Fan, Ross Girshick, and Kaiming He. Improved baselines with momentum contrastive learning. *arXiv preprint arXiv:2003.04297*, 2020. 4, 6

[13] Xinlei Chen, Saining Xie, and Kaiming He. An empirical study of training self-supervised vision transformers. In *ICCV*, pages 9640–9649, 2021. 1, 2, 3, 6

[14] Timothée Darcret, Federico Baldassarre, Maxime Oquab, Julien Mairal, and Piotr Bojanowski. Cluster and predict latent patches for improved masked image modeling. *CoRR*, 2025. 1, 2, 3

[15] Pierre-François De Plaen, Tinne Tuytelaars, Marc Proesmans, and Luc Van Gool. Adversarial dependence minimization. *arXiv preprint arXiv:2502.03227*, 2025. 2

[16] Jia Deng, Wei Dong, Richard Socher, Li-Jia Li, Kai Li, and Li Fei-Fei. Imagenet: A large-scale hierarchical image database. In *CVPR*, pages 248–255. IEEE, 2009. 5, 6

[17] Terrance DeVries and Graham W Taylor. Improved regularization of convolutional neural networks with cutout. *arXiv preprint arXiv:1708.04552*, 2017. 1, 4

[18] Carl Doersch and Andrew Zisserman. Multi-task self-supervised visual learning. In *ICCV*, pages 2051–2060, 2017. 3

[19] Carl Doersch, Abhinav Gupta, and Alexei A Efros. Unsupervised visual representation learning by context prediction. In *ICCV*, pages 1422–1430, 2015. 2

[20] Alexey Dosovitskiy, Lucas Beyer, Alexander Kolesnikov, Dirk Weissenborn, Xiaohua Zhai, Thomas Unterthiner, Mostafa Dehghani, Matthias Minderer, Georg Heigold, Sylvain Gelly, Jakob Uszkoreit, and Neil Houlsby. An image is worth 16x16 words: Transformers for image recognition at scale. In *ICLR*, 2021. 2, 6

[21] Aleksandr Ermolov, Aliaksandr Siarohin, Enver Sangineto, and Nicu Sebe. Whitening for self-supervised representation learning. In *ICML*, pages 3015–3024. PMLR, 2021. 2

[22] Xinyang Geng, Hao Liu, Lisa Lee, Dale Schuurmans, Sergey Levine, and Pieter Abbeel. Multimodal masked autoencoders learn transferable representations. *arXiv preprint arXiv:2205.14204*, 2022. 3

[23] Spyros Gidaris, Praveer Singh, and Nikos Komodakis. Unsupervised representation learning by predicting image rotations. In *ICLR*, 2018. 2

[24] Priya Goyal, Piotr Dollár, Ross Girshick, Pieter Noordhuis, Lukasz Wesolowski, Aapo Kyrola, Andrew Tulloch, Yangqing Jia, and Kaiming He. Accurate, large mini-batch sgd: Training imagenet in 1 hour. *arXiv preprint arXiv:1706.02677*, 2017. 6

[25] Jean-Bastien Grill, Florian Strub, Florent Altché, Corentin Tallec, Pierre Richemond, Elena Buchatskaya, Carl Doersch, Bernardo Avila Pires, Zhaohan Guo, Mohammad Gheshlaghi Azar, et al. Bootstrap your own latent-a new approach to self-supervised learning. *NeurIPS*, 33:21271–21284, 2020. 1, 2, 3, 6, 8, 13

[26] Kaveh Hassani and Mike Haley. Unsupervised multi-task feature learning on point clouds. In *ICCV*, pages 8160–8171, 2019. 3

[27] Kaiming He, Xiangyu Zhang, Shaoqing Ren, and Jian Sun. Deep residual learning for image recognition. In *CVPR*, pages 770–778, 2016. 5, 6

[28] Kaiming He, Haoqi Fan, Yuxin Wu, Saining Xie, and Ross Girshick. Momentum contrast for unsupervised visual representation learning. In *CVPR*, pages 9729–9738, 2020. 1, 2, 3, 6

[29] Kaiming He, Xinlei Chen, Saining Xie, Yanghao Li, Piotr Dollár, and Ross Girshick. Masked autoencoders are scalable vision learners. In *CVPR*, pages 16000–16009, 2022. 1, 2, 6, 7

[30] Sergey Ioffe and Christian Szegedy. Batch normalization: Accelerating deep network training by reducing internal covariate shift. In *ICML*, pages 448–456. PMLR, 2015. 6

[31] Muhammad Abdullah Jamal and Omid Moharer. Multi-modal contrastive masked autoencoders: A two-stage progressive pre-training approach for rgbd datasets. In *CVPR*, pages 17947–17957, 2025. 3

[32] Diederik P Kingma. Adam: A method for stochastic optimization. *arXiv preprint arXiv:1412.6980*, 2014. 6

[33] Tim Lebailly and Tinne Tuytelaars. Global-local self-distillation for visual representation learning. In *WACV*, pages 1441–1450, 2023. 3

[34] Kuang-Huei Lee, Anurag Arnab, Sergio Guadarrama, John Canny, and Ian Fischer. Compressive visual representations. *NeurIPS*, 34:19538–19552, 2021. 6, 13

[35] Timothy P Lillicrap, Jonathan J Hunt, Alexander Pritzel, Nicolas Heess, Tom Erez, Yuval Tassa, David Silver, and Daan Wierstra. Continuous control with deep reinforcement learning. *arXiv preprint arXiv:1509.02971*, 2015. 6

[36] Lilang Lin, Sijie Song, Wenhan Yang, and Jiaying Liu. Ms2l: Multi-task self-supervised learning for skeleton based action recognition. In *Proceedings of the 28th ACM international conference on multimedia*, pages 2490–2498, 2020. 3

[37] Markus Marks, Manuel Knott, Neehar Kondapaneni, Elijah Cole, Thijs Defraeye, Fernando Perez-Cruz, and Pietro Perona. A closer look at benchmarking self-supervised pre-training with image classification. *IJCV*, pages 1–13, 2025. 7

[38] Shlok Mishra, Anshul Shah, Ankan Bansal, Abhyuday Jagannatha, Janit Anjaria, Abhishek Sharma, David Jacobs, and Dilip Krishnan. Object-aware cropping for self-supervised learning. *arXiv preprint arXiv:2112.00319*, 2021. 3

[39] Suhong Moon, Domas Buracas, Seunghyun Park, Jinkyu Kim, and John Canny. An embedding-dynamic approach to self-supervised learning. In *WACV*, pages 2750–2758, 2023. 2, 3

[40] Warren Morningstar, Alex Bijamov, Chris Duvarney, Luke Friedman, Neha Kalibhat, Luyang Liu, Philip Mansfield, Renan Rojas-Gomez, Karan Singhal, Bradley Green, et al. Augmentations vs algorithms: What works in self-supervised learning. *arXiv preprint arXiv:2403.05726*, 2024. 1, 2, 3, 4

[41] Théo Moutakanni, Maxime Oquab, Marc Szafraniec, Maria Vakalopoulou, and Piotr Bojanowski. You don't need domain-specific data augmentations when scaling self-supervised learning. *NeurIPS*, 37:116106–116125, 2024. 3, 8

[42] Mehdi Noroozi and Paolo Favaro. Unsupervised learning of visual representations by solving jigsaw puzzles. In *ECCV*, pages 69–84. Springer, 2016. 2

[43] Maxime Oquab, Timothée Darcet, Théo Moutakanni, Huy Vo, Marc Szafraniec, Vasil Khalidov, Pierre Fernandez, Daniel Haziza, Francisco Massa, Alaaeldin El-Nouby, et al. Dinov2: Learning robust visual features without supervision. *arXiv preprint arXiv:2304.07193*, 2023. 1, 8

[44] Deepak Pathak, Philipp Krahenbuhl, Jeff Donahue, Trevor Darrell, and Alexei A Efros. Context encoders: Feature learning by inpainting. In *CVPR*, pages 2536–2544, 2016. 2

[45] Oriane Siméoni, Huy V Vo, Maximilian Seitzer, Federico Baldassarre, Maxime Oquab, Cijo Jose, Vasil Khalidov, Marc Szafraniec, Seungeun Yi, Michaël Ramamonjisoa, et al. Dinov3. *arXiv preprint arXiv:2508.10104*, 2025. 1

[46] Azad Singh and Deepak Mishra. Branching out for better byol. In *NeurIPS 2021 Workshop on Self-Supervised Learning: Theory and Practice*, 2021. 3

[47] Yuandong Tian, Xinlei Chen, and Surya Ganguli. Understanding self-supervised learning dynamics without contrastive pairs. In *ICML*, pages 10268–10278. PMLR, 2021. 1, 4

[48] Nenad Tomasev, Ioana Bica, Brian McWilliams, Lars Holger Buesing, Razvan Pascanu, Charles Blundell, and Jovana Mitrovic. Pushing the limits of self-supervised resnets: Can we outperform supervised learning without labels on imagenet? In *First Workshop on Pre-training: Perspectives, Pitfalls, and Paths Forward at ICML 2022*, 2022. 6

[49] Hugo Touvron, Matthieu Cord, Matthijs Douze, Francisco Massa, Alexandre Sablayrolles, and Hervé Jégou. Training data-efficient image transformers & distillation through attention. In *ICML*, pages 10347–10357. PMLR, 2021. 6

[50] Vasilis Vryniotis. How to train state-of-the-art models using torchvision's latest primitives. <https://pytorch.org/blog/how-to-train-state-of-the-art-models-using-torchvision-latest-primitives/>, 2021. 6

[51] Lei Wang, Piotr Koniusz, Tom Gedeon, and Liang Zheng. Adaptive multi-head contrastive learning. In *European Conference on Computer Vision*, pages 404–421. Springer, 2024. 3

[52] Xinlong Wang, Rufeng Zhang, Chunhua Shen, Tao Kong, and Lei Li. Dense contrastive learning for self-supervised visual pre-training. In *CVPR*, pages 3024–3033, 2021. 3

[53] Xiao Wang, Haoqi Fan, Yuandong Tian, Daisuke Kihara, and Xinlei Chen. On the importance of asymmetry for siamese representation learning. In *CVPR*, pages 16570–16579, 2022. 4

[54] Tete Xiao, Colorado J Reed, Xiaolong Wang, Kurt Keutzer, and Trevor Darrell. Region similarity representation learning. In *ICCV*, pages 10539–10548, 2021. 3

[55] Enze Xie, Jian Ding, Wenhui Wang, Xiaohang Zhan, Hang Xu, Peize Sun, Zhenguo Li, and Ping Luo. Detco: Unsupervised contrastive learning for object detection. In *ICCV*, pages 8392–8401, 2021. 3

[56] Zhenda Xie, Zheng Zhang, Yue Cao, Yutong Lin, Jianmin Bao, Zhiliang Yao, Qi Dai, and Han Hu. Simmim: A simple framework for masked image modeling. In *CVPR*, pages 9653–9663, 2022. 2, 6

[57] Jiange Yang, Sheng Guo, Gangshan Wu, and Limin Wang. Comae: Single model hybrid pre-training on small-scale rgbd datasets. In *AAAI*, pages 3145–3154, 2023. 3

[58] Yang You, Igor Gitman, and Boris Ginsburg. Large batch training of convolutional networks. *arXiv preprint arXiv:1708.03888*, 2017. 6

[59] Sangdoo Yun, Dongyoon Han, Seong Joon Oh, Sanghyuk Chun, Junsuk Choe, and Youngjoon Yoo. Cutmix: Regularization strategy to train strong classifiers with localizable features. In *ICCV*, pages 6023–6032, 2019. 3, 14

[60] Jure Zbontar, Li Jing, Ishan Misra, Yann LeCun, and Stéphane Deny. Barlow twins: Self-supervised learning via redundancy reduction. In *ICML*, pages 12310–12320. PMLR, 2021. 1, 2, 6

- [61] Xiaohua Zhai, Avital Oliver, Alexander Kolesnikov, and Lucas Beyer. S4l: Self-supervised semi-supervised learning. In *ICCV*, pages 1476–1485, 2019. [13](#)
- [62] Hongyi Zhang, Moustapha Cisse, Yann N Dauphin, and David Lopez-Paz. mixup: Beyond empirical risk minimization. *arXiv preprint arXiv:1710.09412*, 2017. [3](#)
- [63] Richard Zhang, Phillip Isola, and Alexei A Efros. Colorful image colorization. In *ECCV*, pages 649–666. Springer, 2016. [2](#)
- [64] Tong Zhang, Congpei Qiu, Wei Ke, Sabine Süsstrunk, and Mathieu Salzmann. Leverage your local and global representations: A new self-supervised learning strategy. In *CVPR*, pages 16580–16589, 2022. [2](#)
- [65] Zhun Zhong, Liang Zheng, Guoliang Kang, Shaozi Li, and Yi Yang. Random erasing data augmentation. In *AAAI*, pages 13001–13008, 2020. [3](#)
- [66] Jinghao Zhou, Chen Wei, Huiyu Wang, Wei Shen, Cihang Xie, Alan Yuille, and Tao Kong. Image bert pre-training with online tokenizer. In *ICLR*, 2021. [2](#)

# Supplementary Material

## A. Experimental Settings

In this section, we detail the implementation settings required to reproduce the results reported in Secs. 4.1 to 4.4, 5.1 and 5.2. Unless specified otherwise, all experiments use ResNet-50 backbones, the standard ImageNet-1k training/validation splits, and synchronized batch normalization. All models are trained from scratch without labels, using mixed-precision training on a single 4×Nvidia A100 GPU node.

**BYOL and MoCo v3 baselines.** We closely follow the official training recipes for both methods, which use nearly identical hyperparameters. We pre-train ResNet-50 backbones with two-layer projection and prediction heads, each with a hidden dimension of 4096 and an output dimension of 256. All heads use intermediate batch normalization and ReLU activations. For MoCo v3, we additionally apply batch normalization on the outputs of both heads, following the official implementation. We pre-train the baselines for 200 epochs using the LARS optimizer, a linearly scaled learning rate (base value 0.4), a cosine decay schedule applied per training step, and a 10-epoch warm-up. For both methods, the target network is updated using an EMA of the online networks, with a momentum coefficient following a cosine schedule from 0.996 to 1.0. All experiments use a batch size of 1024.

**SimSiam baseline.** For SimSiam, we again follow the original training recipe. The projection layer is a three-layer MLP with hidden and output dimensions of 2048, and the prediction head is a two-layer bottleneck MLP with a hidden dimension of 512 and an output dimension of 2048. Both heads use intermediate batch normalization and ReLU activations, and the projection head additionally uses batch normalization on its output. We pre-train the baseline for 200 epochs with the SGD optimizer, a linearly scaled learning rate (base value 0.05), a batch size of 512, a cosine decay schedule applied per epoch, and no warmup. The prediction head uses a constant learning rate, as in the original paper.

**Base data augmentations.** We adopt the official data augmentation strategies from the respective methods. Unless stated otherwise, training views are obtained by applying the following sequence of transformations:

1. random resized cropping: a random patch of the image is selected, with an area uniformly sampled between 8%

and 100% of that of the original image, and an aspect ratio logarithmically sampled between 3/4 and 4/3. For SimSiam and MoCo v3, the minimum area is set to 20%.

2. random horizontal flipping with a probability of 50%.
3. random color jitter: brightness, contrast, saturation, and hue are perturbed with random offsets uniformly sampled for each image. BYOL and MoCo v3 use the ranges (0.4, 0.4, 0.2, 0.1), while SimSiam uses (0.4, 0.4, 0.4, 0.1).
4. random grayscale with a probability of 20%.
5. random Gaussian blur: the image is blurred with a Gaussian blur kernel of size 23 and a standard deviation uniformly sampled in [0.1, 2]. In BYOL and MoCo v3, the transformation is applied with 100% probability for the first view and 10% for the second; in SimSiam, both views use a 50% probability.
6. random solarization with probability 20% in the second view, for BYOL and MoCo v3.
7. color normalization: finally, we normalize the color channels by subtracting the per-channel mean and dividing by the per-channel standard deviation estimated on the ImageNet training set.

**Multi-predictor multi-crop and multi-task strategies.** All multi-crop and multi-task experiments reuse the hyperparameters of their respective 2-view baselines to ensure a strictly controlled comparison. The multi-crop experiments use two global views and four local views, and the multi-task runs use two global, two local, and one cutout view. Following previous works [8, 9], local crops have a resolution of 96×96, with the random crop area sampled in the interval [0.08, 0.25]. Global and cutout crops have a resolution of 224×224, with the random crop area sampled in the interval [0.25, 1.0]. The two global views follow BYOL’s base data augmentation setting described above. For local and cutout views, we apply random horizontal flipping with probability 50%, color jitter with BYOL’s parameter ranges, random grayscale with probability 20%, and Gaussian blur with probability 50%.

**Random cutout.** Our random cutout implementation follows the hyperparameter sampling strategy of Torchvision’s `RandomResizedCrop`. We uniformly sample a cutout area between 20% and 40% of the original image area, and an aspect ratio logarithmically sampled between 3/4 and 4/3. The selected region is masked with a constant fill value equal to the ImageNet mean color, so that the masked pixels have an expected value of zero after color normalization.

Method	Top-1		Top-5	
	1%	10%	1%	10%
supervised	25.4	56.4	48.4	80.4
SimCLR	<b>48.3</b>	<b>65.6</b>	<b>75.5</b>	<b>87.8</b>
BYOL	53.2	68.8	78.4	89.0
SwAV	53.9	70.2	78.5	89.9
Barlow Twins	55.0	69.7	79.2	89.3
NNCLR	56.4	69.8	80.7	89.3
C-BYOL	<b>60.6</b>	70.5	83.4	90.0
ReLIC v2	58.1	72.4	81.3	91.2
BYOL multi-task	60.4	<b>72.5</b>	<b>84.0</b>	<b>91.3</b>

Table 7. Semi-supervised training on ImageNet-1k with 1% and 10% of labels. We report top-1 and top-5 validation set accuracies.

**Ablation Study on Data Augmentations.** In the ablation on data augmentations, all experiments reuse the optimization hyperparameters of the 200-epoch BYOL baseline. We vary only the set of augmentations applied during pre-training.

**kNN evaluation.** For kNN evaluation, we follow the standard protocol used in prior work on self-supervised learning. Each image is resized to a shorter side of 256 pixels and then center-cropped to  $224 \times 224$  before feature extraction. For each validation sample, we retrieve its top-20 nearest neighbors in the feature space using cosine similarity, and predict the label by a simple majority vote among them.

**Linear evaluation.** For linear probing, a linear classifier is trained on top of the frozen backbone features. To eliminate the need for per-model learning rate tuning, feature vectors are standardized using mean and variance statistics computed on ImageNet. For ResNet 50 architectures, features are extracted after the global average pooling layer, before the projection head. For Vision Transformers (ViT), the extraction protocol follows DINO [9]. For ViT S, features consist of the concatenated [CLS] tokens from the final four layers. For ViT B, features are formed by concatenating the [CLS] token with the global average-pooled output patch tokens. We train the linear head for 100 epochs with the SGD optimizer, a learning rate of 0.005, a batch size of 512, no weight decay, and a cosine learning rate schedule. During training, we apply random horizontal flipping with probability 50% and random cropping that keeps at least 8% of the image area, followed by resizing to  $224 \times 224$  pixels. At evaluation time, images are resized so that the shorter side is 256 pixels, then center-cropped to  $224 \times 224$  pixels.

Method	Top-1	Top-5
SimCLR	76.0	93.1
BYOL	77.7	93.7
BYOL multi-task	<b>79.3</b>	<b>94.8</b>

Table 8. Fine-tuning on ImageNet-1k with neither heavy data augmentations nor regularization.

## B. Additional Evaluations

**Semi-supervised learning.** We follow the semi-supervised learning protocol from [10, 25, 61], which we describe next for completeness. We fine-tune the pre-trained ResNet-50 backbone from Sec. 4.4 using subsets of ImageNet-1k labels (1% and 10%), as provided by Chen et al. [10]. During training, we apply the same data augmentations as for linear evaluation: random horizontal flipping and random cropping (with scales in the range 0.08-1), followed by resizing to  $224 \times 224$  pixels. At test time, images are resized to 256 pixels along the shorter side using bicubic resampling, followed by a center crop to  $224 \times 224$  pixels. In all cases, we use the same color normalization as during pre-training. We attach a linear classification head to the backbone and train the network with a softmax cross-entropy loss using SGD with Nesterov momentum 0.9, a batch size of 1024, and no additional regularization (e.g., no weight decay). We sweep over learning rate values in  $\{0.005, 0.01, 0.02, 0.05, 0.1\}$  and training schedules of 30 and 50 epochs, and report the test accuracy of the best configuration in Tab. 7. Our approach significantly outperforms BYOL and achieves state-of-the-art performance. In the 1% setting, it outperforms ReLIC v2 by a large margin and matches the performance of C-BYOL [34], a compressive variant of BYOL. Notably, the C-BYOL objective could in principle be combined with our augmentation strategy, which we leave for future work.

**Fine-tuning.** We also fine-tune the pre-trained models on the full ImageNet-1k training set using the same simple protocol, with only two data augmentations and no explicit regularization. As reported in Tab. 8, our BYOL multi-task variant improves over standard BYOL by +1.6 points in top-1 accuracy and by +1.1 points in top-5 accuracy.

## C. Timing Analysis

Tab. 9 compares training cost and wall-clock efficiency across different BYOL training strategies. Although multi-task training increases the per-epoch cost, it is much more wall-clock efficient. The 200-epoch multi-task model (72h) outperforms the 1000-epoch baseline (219h) by 1.3% accuracy, corresponding to an approximately  $3 \times$  gain in training efficiency.

Furthermore, the method is implemented with per-view forward and backward passes, keeping memory usage independent of the number of views. This reordering is mathematically equivalent to the standard multi-view formulation, yielding identical gradients. Under this setup, peak per-GPU memory consumption is 12.7 GB for all three augmentation strategies.

Strategy	Epochs	Time/Ep	Total (h)	Acc.
baseline	200	13:09	44	70.7
multi-pred m-c	200	19:51	66	74.7
multi-task	200	21:35	72	<b>75.6</b>
baseline	1000	13:09	219	74.3

Table 9. Training efficiency on BYOL (ResNet-50) using a single node with 4× Nvidia A100 (80GB) GPUs. Multi-pred m-c uses 2 global and 4 local views; multi-task uses 2 global, 2 local, and 1 cutout view.

## D. Negative Results and Future Directions

While augmenting the multi-crop strategy with cutout views yielded significant gains (Tab. 5), several alternative spatial and mixing transformations proved ineffective. To guide the development of future work, we detail the online view-generation strategies that failed to improve performance:

- **Random Rotation:** Applying stochastic rotations to the input image before cropping.
- **Patch Shuffling:** Dividing the input into a grid of patches (similar to Vision Transformer tokenization) and performing a random shuffle.
- **CutMix-like:** Adopting a CutMix [59] approach where the online branch processes a blended image. The corresponding target was defined as a weighted average of the individual representations (passed separately to the target branch).

The first two strategies yielded marginal gains that did not justify the increased computational overhead, while the third degraded performance.

An alternative approach for *Random Rotation* or *Patch Shuffling* would be to provide a conditioning signal to the predictors (e.g., the specific rotation angle). This modification would transform the method from a standard Siamese or Joint-Embedding Architecture into a Joint-Embedding Predictive Architecture, shifting the focus from learning invariant features to task-conditional prediction and enabling richer forms of self-supervision.